

MAMO: Masked Multimodal Modeling for Fine-Grained Vision-Language Representation Learning

Zijia Zhao^{†*1,2,3}, Longteng Guo^{†2}, Xingjian He^{1,3}, Shuai Shao², Zehuan Yuan², Jing Liu^{‡1,3}

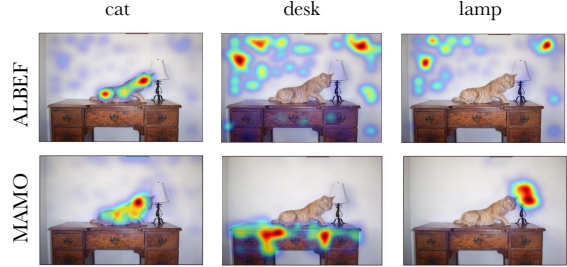
¹National Laboratory of Pattern Recognition, Institute of Automation, Chinese Academy of Sciences

²Bytedance Inc ³ University of Chinese Academy of Sciences

zhaozijia2021@ia.ac.cn, {xingjian.he, jliu}@nlpr.ia.ac.cn,
 {guolongteng.lt, shaoshuai.0516, yuanzehuan}@bytedance.com

Abstract

Multimodal representation learning has shown promising improvements on various vision-language tasks. Most existing methods excel at building global-level alignment between vision and language while lacking effective fine-grained image-text interaction. In this paper, we propose a jointly masked multimodal modeling method to learn fine-grained multimodal representations. Our method performs joint masking on image-text input and integrates both implicit and explicit targets for the masked signals to recover. The implicit target provides a unified and debiased objective for vision and language, where the model predicts latent multimodal representations of the unmasked input. The explicit target further enriches the multimodal representations by recovering high-level and semantically meaningful information: momentum visual features of image patches and concepts of word tokens. Through such a masked modeling process, our model not only learns fine-grained multimodal interaction, but also avoids the semantic gap between high-level representations and low- or mid-level prediction targets (e.g. image pixels), thus producing semantically rich multimodal representations that perform well on both zero-shot and fine-tuned settings. Our pre-trained model (named MAMO) achieves state-of-the-art performance on various downstream vision-language tasks, including image-text retrieval, visual question answering, visual reasoning, and weakly-supervised visual grounding.



Caption: a **cat** on the **desk** near a **lamp**

Figure 1. Per-word Grad-CAM visualization of word to image attention. Comparing with ALBEF [19], MAMO can focus on corresponding region for each word more precisely, indicating more fine-grained interactions between word and image patches are built. More examples can be seen in Appendix.

1. Introduction

Vision-Language Pre-training (VLP) aims to learn the interaction between image and text and produce semantically rich multimodal representations that transfer well to downstream Vision-and-Language (V+L) tasks. In order to learn cross-modal interaction, most existing VLP methods [5, 15, 19, 21, 28, 33] rely on the consistency between the global views of image and text, using pre-training objectives like image-text contrastive loss [19] and image-text matching loss [33]. While effective, such global interaction fails to model the subtle local association within image-text pairs. The fine-grained interaction between image patches and word tokens is therefore lacking.

Masked signal modeling is an effective self-supervised pre-training task that masks a portion of input signals and tries to predict these masked signals from the visible ones. It has been actively explored in natural language processing (NLP) and computer vision (CV) separately, and has brought powerful generalization performance across diverse

[†]Equal contribution.

[‡]Corresponding author.

*This work was performed while Zijia worked as an intern at ByteDance.

downstream tasks. For example, BERT [17] formulates masked language modeling (MLM) to predict masked linguistic tokens, while MAE [14] and BEiT [2] formulate masked image modeling (MIM) to reconstruct raw pixels and dVAE visual tokens [29] of image patches respectively. In the domain of VLP, however, there is a lack of a jointly masked signal modeling method for both vision and language modalities. Although previous VLP methods [5, 19] have adopted conditional MLM to predict masked words given *unmasked* image and other words, however, masking of the image side has not been fully explored. As a result, the images’ internal structures and their interactions with text tokens are not sufficiently learned, as is shown in Fig. 1.

The challenge of designing a jointly masked signal modeling method for VLP lies in the natural differences between image and text modalities — image is continuous, low-level, highly redundant raw signals, while text tokens are discrete, high-level, highly compressed concepts generated by humans. This phenomenon raises two questions: (1) How to design a unified prediction target that applies to masked multimodal data composing both continuous visual signals and discrete text tokens? (2) How to avoid the semantic gap between the learning of high-level representations and the prediction of low-level image signals?

In this paper, we propose MAsked Multimodal mOdel (MAMO), a VLP model with a jointly masked learning strategy on both vision and language modalities. MAMO performs joint masking on image-text input and integrates both implicit and explicit targets for the masked signals to recover. The *implicit* target provides a unified and debiased objective for vision and language, the core idea of which is to predict latent multimodal representations of the masked signals under the guidance of a self-distillation teacher that takes the unmasked view as input. Such a bootstrapping latent target avoids learning biases in modality-specific designs. While the implicit prediction target performs effective empirically, it can collapse into meaningless solutions, *e.g.*, outputting the same vector for all tokens. To further enrich the multimodal representations and avoid such potential trivial solutions, we also add auxiliary *explicit* prediction targets that are naturally distinguishable on each masked position. These targets are explicit in that they are semantically meaningful features or concepts extracted from the raw data. Particularly, for the masked image tokens, instead of reconstructing low-level raw pixels [14] or predicting mid-level pre-defined visual tokens [2] (encapsulating mostly patch details, *e.g.* color and texture, according to [42]), they are enforced to predict the high-level momentum visual features extracted from the image encoder. As for masked text tokens, we directly predict word tokens since they are already high-level concepts.

MAMO naturally addresses the aforementioned two questions: First, the prediction targets of both masked vi-

sion and language signals are unified as regressing the implicit latent multimodal representations; Second, our implicit and explicit prediction targets are both high-level representations and features/concepts, thus avoiding the semantic-gap caused by predicting low- or mid-level image signals. Such a masked modeling process enforces the model to build both intra- and inter-modality interactions between image patches and word tokens, and produce fine-grained and semantically rich multimodal representations that perform well on both zero-shot and fine-tuned settings.

We demonstrate the effectiveness of MAMO on various downstream V+L tasks including image-text retrieval, visual question answering, visual reasoning, and weakly-supervised visual grounding. MAMO achieves substantial improvements over existing state-of-the-art methods. On zero-shot image-text retrieval, MAMO even outperforms methods that are pre-trained on orders of magnitude larger datasets, *e.g.*, it outperforms the state-of-the-art methods, CLIP [28] and ALIGN [15], by absolute improvements of 9.4% and 2.4% on image retrieval R@1, respectively. Quantitative and qualitative analyses on MAMO using Grad-CAM [31] further demonstrate its ability to perform more fine-grained vision-language interaction.

Our contributions are summarized as follows:

- We propose a jointly masked multimodal modeling method that integrates both implicit and explicit prediction targets to learn fine-grained multimodal representations.
- Our implicit target provides a unified and debiased objective for VLP, and our explicit target shows that high-level momentum visual features can serve as a better auxiliary target for masked images compared with low-level pixels or mid-level visual tokens.
- Qualitative and quantitative results across a broad range of downstream tasks show that our method learns fine-grained and transferable vision-language representations.

2. Related Work

2.1. Vision-Language Representation Learning

Depending on how vision and language modalities interact, most previous VLP methods fall into two categories: shallow interaction and deep interaction. Shallow interaction methods [15, 28] use light-weight operations (*e.g.*, dot product) for interaction while deep interaction methods [5, 20, 21, 33, 35, 41] use deep networks (*e.g.*, a transformer-based multimodal encoder) to fuse image and text features. ALBEF [19] combines the above two types of methods, learning both shallow and deep interactions in a single framework. To train such interaction networks, previous VLP methods often employ contrastive learning [19]

or image-text matching [20] as pre-training tasks, which excel at learning global-level image-text alignment, but lack effective modeling of fine-grained interaction between image patches and word tokens. MAMO inherits the architecture of ALBEF to combine shallow and deep interactions and further introduces a new masked multimodal modeling method to enforce fine-grained multimodal interaction.

2.2. Masked Signal Modeling

Masked signal modeling has been actively explored in NLP and CV separately. The prediction target for masked signals to recover is one of the main differences in previous works. In NLP, word token is the most commonly used prediction target. In CV, various targets are explored, *e.g.*, raw pixel [14, 37], HOG features [36], visual tokens [2] from a pre-trained dVAE [29], visual tokens from a momentum model [42], *etc.*

In VLP, conditional MLM is a commonly used pre-training objective, which predicts masked text tokens based on unmasked images. Some works perform MIM in VLP. UNITER [5] applies masking on pre-extracted regional features and let the model predict the class label or feature of those regions. OSCAR [21] inputs additional object tags into the model and adds a mask-and-predict task on these object tags. However, these methods require a pre-trained model, *e.g.*, object detector like Faster R-CNN [30], to extract the prediction target, causing domain bias and error propagation. Most recently, inspired by MAE [14], several concurrent works, *e.g.*, M3AE [10] and VLC [13], transfer the pixel reconstruction task into VLP by simply adding pixel reconstruction tasks on top of VLP models. These VLP methods, however, neglect the semantic gap between low-level pixels (or mid-level visual tokens) and high-level multimodal representations, which can disturb the learning of semantically rich representations. Our MAMO unifies masked multimodal modeling of both vision and language as predicting the high-level latent representations and features/concepts, thus avoiding the potential negative impacts brought by the semantic gaps.

2.3. Self-Distillation

Self-distillation methods [3, 12] attempt to utilize history knowledge to drive the model learning from itself. BYOL [12] proposes a self-supervised image representation learning approach that iteratively bootstraps the outputs of a network to serve as targets for enhanced representations. Some methods [1, 42] combine this learning strategy with masked modeling for separate modalities. The implicit prediction target of MAMO gets inspiration from these methods, but our work differs in that we operate on multimodal inputs and representations, and further enhance the representations with the aid of explicit and semantically meaningful targets.

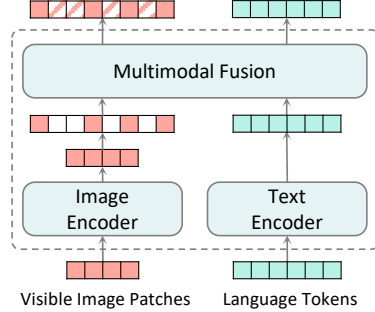


Figure 2. Architecture of MAMO.

3. Method

3.1. Model Architecture

As illustrated in Fig. 2, our model includes an image encoder, a text encoder, and a multimodal fusion encoder. The image encoder is a pre-trained visual transformer, ViT-B/16 [8]. The text encoder and the multimodal fusion encoder are both based on transformer, which are initialized with the first 6 layers and the last 6 layers of BERT_{base} [17], respectively. The image encoder encodes an input image I into a sequence of visual features $\{v_{cls}, v_1, v_2, \dots, v_N\}$, where v_{cls} represents the global feature on the [CLS] token and others correspond to each visible image patch. Particularly, we append a shared, learnable vector (*i.e.*, mask token) into those visual features to indicate the presence of a missing patch to be predicted, and add positional embeddings to all tokens in this full set. The text encoder transforms an input text T into a sequence of linguistic token features $\{w_{cls}, w_1, w_2, \dots, w_N\}$. The visual and linguistic tokens are concated and fed to the multimodal fusion encoder to generate fused multimodal representations.

3.2. Pre-training Tasks

We pre-train our model with two categories of pre-training tasks: 1) masked multimodal modeling, which enables learning fine-grained multimodal interaction by the way of mask-and-predict; 2) global-level image-text alignment, which aligns image and text from the perspective of their global consistency.

3.2.1 Masked Multimodal Modeling

Masked multimodal modeling is designed to learn fine-grained multimodal interaction for vision-language input. Given an image-text pair (I, T) , we create two masked views, (\hat{I}, T) and (I, \hat{T}) , by randomly masking a portion of the input, *i.e.*, either removing some image patches or replacing some sub-words in the text with [MASK] token. The masked views, (\hat{I}, T) and (I, \hat{T}) , are sent into our model, the online network f parameterized by θ , to get their multimodal representations, $f_\theta(\hat{I}, T)$ and $f_\theta(I, \hat{T})$. We then

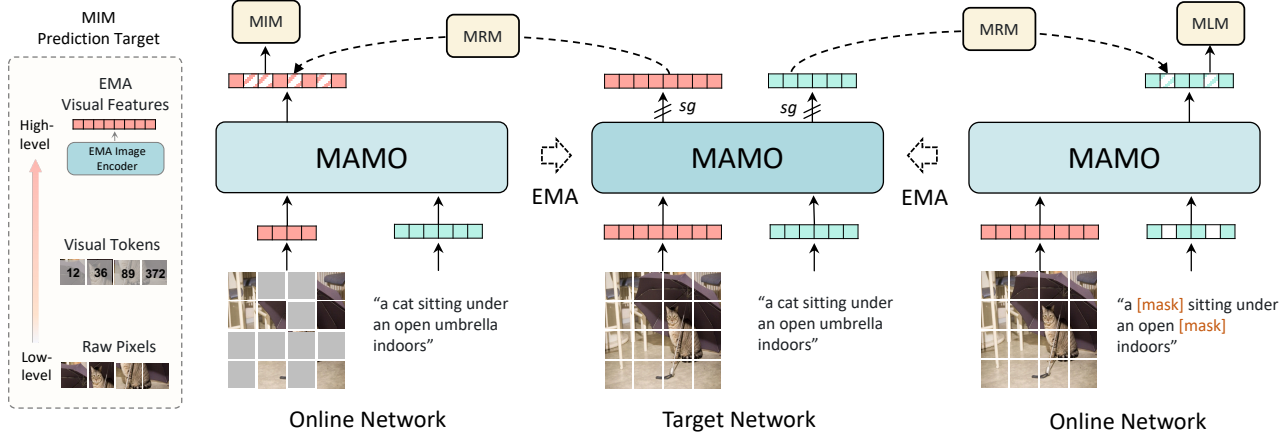


Figure 3. Illustration of our masked multimodal modeling method. We enforce fine-grained multimodal interaction by jointly performing mask-and-predict tasks on both vision and language. MRM is an implicit, unified prediction target for vision and language that performs self-distillation between the online network and an exponentially moving averaged (EMA) target network. MIM and MLM are explicit, semantically meaningful prediction targets for image and text respectively. sg means stop gradient.

design an implicit (masked representation modeling) and two explicit (masked image/language modeling) prediction sub-tasks for those masked views.

Masked Representation Modeling (MRM). MRM serves as an implicit, unified, and debiased prediction target for both vision and language. It requires predicting latent multimodal representations on each masked position under the guidance of a self-distillation teacher, which is referred to as the target network.

The target network has the same architecture as the online network, both defined as f , but uses a different set of parameters. We don't simply copy the online network to the target network because the frequent change in the target network makes the learning process diverge. To acquire a smoothing target, we utilize a momentum target network [12] whose parameters $\bar{\theta}$ are updated by an exponential moving average (EMA) of the online parameters θ : $\bar{\theta} \leftarrow \alpha\bar{\theta} + (1 - \alpha)\theta$. We stop the gradient propagation in the target network.

We send the unmasked raw input (I, T) into the target network to get its latent multimodal representation $f_{\bar{\theta}}(I, T)$. This full, unmasked representation then serves as the prediction target of $f_{\theta}(\hat{I}, T)$ and $f_{\theta}(I, \hat{T})$ on masked positions. Following [4], we add a non-linear projector g on both the online and target networks, which have been empirically shown beneficial to performance according to [4]. We here define the MRM objective as:

$$\mathcal{L}_{mrm} = \mathbb{E}_{(I, T) \sim D} \left[\ell_{mrm} \left(f_{\theta}(I, \hat{T}), f_{\bar{\theta}}(I, T) \right) + \ell_{mrm} \left(f_{\theta}(\hat{I}, T), f_{\bar{\theta}}(I, T) \right) \right] \quad (1)$$

The objective function $\ell_{mrm}(x, y)$ calculates mean squared error (MSE) between predictions $h_{mrm} \circ g_{\theta}(x)$ and targets $g_{\bar{\theta}}(y)$ on each masked position. The projector g and the predictor h_{mrm} are both MLPs with one hidden layer.

MRM unifies the training objective of both vision and language, and avoids learning biases in modality-specific designs. Our momentum representation targets can be seen as a dynamic ensemble of historical targets, which offers varying target views that encourage the online network learning more general semantic representations.

While MRM is effective empirically, such self-distillation may collapse into trivial solutions, *e.g.*, outputting the same vector for all masked positions. To overcome such problems and further enrich the multimodal representations, we then introduce two explicit and semantically meaningful prediction targets for vision and language, respectively.

Masked Image Modeling (MIM). MIM feeds (\hat{I}, T) into the network, and predicts the masked image information with the help of the text and the visible image patches. In self-supervised learning of images, popular MIM targets include raw pixels [14, 37], visual tokens [2] from a pre-trained dVAE [29], *etc.*, as are displayed in the left side of Fig. 3. However, pixels are low-level raw signals containing high-frequency details, while visual tokens [2] are mid-level information that encapsulating mostly patch details (*e.g.* color and texture, according to [42]). Such low- and mid-level prediction targets have semantic gaps with high-level representations. Learning of such targets makes the model struggle in separating semantics and visual details, yielding less competitive performance in semantic understanding [23]. Also, the visual tokens rely on an offline

pre-trained dVAE [29] model, which may result in error propagation.

In replacement of these previous image prediction targets, we introduce the momentum visual features, extracted by the target network’s image encoder f_θ^v , to be a more appropriate prediction target of MIM in VLP. The momentum visual features are high-level and semantically meaningful, thus can avoid the aforementioned semantic gap. Our MIM objective can be formulated as:

$$\mathcal{L}_{mim} = \mathbb{E}_{(I, T) \sim D} \ell_{mim} \left(f_\theta(\hat{I}, T), f_\theta^v(I, T) \right) \quad (2)$$

The objective function $\ell_{mim}(x, y)$ calculates L1 loss between predictions $h_{mim}(x)$ and targets y on each masked image position, where h_{mim} denotes an MLP predictor.

Masked Language Modeling (MLM). MLM feeds (I, \hat{T}) into the network, and predicts the masked text information. Since word concepts in the text are already information-dense and semantically rich, we simply use word tokens as the explicit target, which is as same as the masked language modeling in [17]. MLM predicts original word tokens on each masked text position. The MLM objective is defined as:

$$\mathcal{L}_{mlm} = \mathbb{E}_{(I, T) \sim D} \ell_{mlm} \left(f_\theta(I, \hat{T}), T \right) \quad (3)$$

The objective function $\ell_{mlm}(x, y)$ calculates cross-entropy loss between word prediction probability $h_{mlm}(x)$ and the ground-truth y on each masked text position, where h_{mlm} denotes a linear-softmax predictor.

3.2.2 Global-level Image-Text Alignment

Global-level image-text alignment is designed to learn global consistency between image and text from perspectives of unimodal and multimodal representations, respectively.

Image-Text Contrastive Learning (ITC). ITC [19] facilitates the global alignment between the features of images and their corresponding texts before feeding them into the multimodal fusion encoder. Given a batch of image-text pairs $\{(I_j, T_j)\}_{j=1}^N$, ITC minimizes the InfoNCE [25] loss as:

$$\mathcal{L}_{itc} = -\frac{1}{2} \mathbb{E}_{(I, T) \sim D} \left[\log \frac{\exp(s(I, T)/\tau)}{\sum_{j=1}^N \exp(s(I, T_j)/\tau)} + \log \frac{\exp(s(I, T)/\tau)}{\sum_{j=1}^N \exp(s(I_j, T)/\tau)} \right] \quad (4)$$

where $s(I, T) = g^v(v_{cls})^\top g^t(w_{cls})$ is the similarity function, g^v and g^t denote two projection heads and τ is a learnable temperature parameter [28].

Image-Text Matching Learning (ITM). ITM aims to determine whether an image and a text are matched. We use the similarity probability in ITC to sample an in-batch hard negative example for each image and each text respectively. And then, we use the [CLS] token from multimodal fusion encoder’s output to predict whether the given image-text pair is matched. The ITM loss is defined as:

$$\mathcal{L}_{itm} = \mathbb{E}_{(I, T) \sim D} \ell_{itm} (f_\theta(I, T), y(I, T)) \quad (5)$$

The objective function $\ell_{itm}(x, y)$ calculates the cross-entropy loss between the matching probability $p(x_{cls})$ and the matching label y for each sample.

Finally, the full pre-training objective of MAMO is:

$$\mathcal{L} = \mathcal{L}_{mrm} + \mathcal{L}_{mim} + \mathcal{L}_{mlm} + \mathcal{L}_{itc} + \mathcal{L}_{itm} \quad (6)$$

4. Experiments

4.1. Pre-training Datasets

Following previous works [5, 19], we construct our image-text pre-training data using the union of two web datasets, *i.e.*, Conceptual Captions [32] and SBU Captions [26], and two in-domain datasets, *i.e.*, Visual Genome [18] and MSCOCO Captions [22]. The total number of unique images is 4.1M, and the number of image-text pairs is 5.2M.

4.2. Implementation Details

Our model consists of a BERT_{base} [17] with 110.1M parameters and a ViT-B/16 [8] with 85.9M parameters. We pre-train the model for 30 epochs using a batch size of 1536 on 16 NVIDIA A100 GPUs. We use the AdamW [24] optimizer with a weight decay of 0.01. The learning rate is warmed-up to 1×10^{-4} in the first 2500 iterations, and decayed to 1×10^{-5} following a linear schedule. During pre-training, we take random image crops of resolution 224×224 as input, and also apply RandAugment [7]. We keep 25% masking ratio on text modality, the replacements are 10% random tokens, 10% unchanged, and 80% [MASK] token. And we apply random masks on image patches with a masking ratio of 75%. Following previous works [9, 19, 38], during fine-tuning, we increase the image resolution to 384×384 and interpolate the positional encodings of image patches following [8]. The momentum parameter α for updating the target network is set as 0.995.

4.3. Downstream Tasks

We mainly apply our pre-trained model to four common V+L downstream tasks. More details on fine-tuning setups are in Appendix.

Image-Text Retrieval includes two sub-tasks: text-to-image retrieval (IR) and image-to-text retrieval (TR). We evaluate the performance on Flickr30K [27] and

Method	#Images	MSCOCO (5k test set)				Flickr30K (1k test set)			
		TR		IR		TR		IR	
		R@1 / R@5 / R@10	R@1 / R@5 / R@10	R@1 / R@5 / R@10	R@1 / R@5 / R@10	R@1 / R@5 / R@10	R@1 / R@5 / R@10	R@1 / R@5 / R@10	R@1 / R@5 / R@10
UNITER _{large} [5]	4M	65.7 / 88.6 / 93.8		52.9 / 79.9 / 88.0		87.3 / 98.0 / 99.2		75.6 / 94.1 / 96.8	
ALBEF [19]	4M	73.1 / 91.4 / 96.0		56.8 / 81.5 / 89.2		94.3 / 99.4 / 99.8		82.8 / 96.7 / 98.4	
TCL [38]	4M	75.6 / 92.8 / 96.7		59.0 / 83.2 / 89.9		94.9 / 99.5 / 99.8		84.0 / 96.7 / 98.5	
CODIS [9]	4M	75.3 / 92.6 / 96.6		58.7 / 82.8 / 89.7		95.1 / 99.4 / 99.9		83.3 / 96.1 / 97.8	
VLC [13]	5.6M	71.3 / 91.2 / 95.8		50.7 / 78.9 / 88.0		89.2 / 99.2 / 99.8		72.4 / 93.4 / 96.5	
ALIGN [15]	1.8B	77.0 / 93.5 / 96.9		59.9 / 83.3 / 89.8		95.3 / 99.8 / 100.0		84.9 / 97.4 / 98.6	
MAMO	4M	77.1 / 94.0 / 97.0		60.3 / 84.0 / 90.4		95.6 / 99.6 / 99.9		85.4 / 97.1 / 98.5	

Table 1. Fine-tuned image-text retrieval results on MSCOCO and Flickr30K datasets. IR: image retrieval. TR: text retrieval.

Method	#Images	Flickr30K (1k test set)			
		TR		IR	
		R@1 / R@5 / R@10	R@1 / R@5 / R@10	R@1 / R@5 / R@10	R@1 / R@5 / R@10
UNITER _{large} [5]	4M	83.6 / 95.7 / 97.7		68.7 / 89.2 / 93.9	
ALBEF [19]	4M	85.2 / 97.5 / 98.9		69.4 / 88.9 / 93.3	
CLIP [28]	400M	88.0 / 98.7 / 99.4		68.7 / 90.6 / 95.2	
ALIGN [15]	1.8B	88.6 / 98.7 / 99.7		75.7 / 93.8 / 96.8	
MAMO	4M	91.3 / 99.2 / 99.8		78.1 / 93.1 / 95.9	

Table 2. Zero-shot image-text retrieval results on Flickr30K. For fair comparison of *real* zero-shot performance, the retrieval results of all methods are from their pre-trained models.

MSCOCO [22] benchmarks on the fine-tuned and zero-shot settings. Some of the previous methods [9, 19, 38] use the model fine-tuned on MSCOCO for zero-shot evaluation on Flickr30K, which although reports better results but cannot validate the real zero-shot capability of the pre-trained model. Therefore, for fair zero-shot evaluation, we directly use the pre-trained model and set the input resolution as the pre-training resolution.

Visual Question Answering (VQA) requires the model to predict an answer given an image and a question. We evaluate our model on VQA2.0 dataset [11]. Following previous methods [6, 19], we first fuse the question and image with our pre-trained model, and then input the multimodal representation sequence to a 6-layer transformer decoder to auto-regressively generate answers.

Natural Language for Visual Reasoning (NLVR) lets the model determine whether a given text describes the relationship between two images. We evaluate our model on NLVR2 dataset [34]. Following [5], we create two image-text pairs using the same text and different images, and get their respective multimodal representations. And then we use bidirectional attention to establish interactions between the two outputs.

Visual Grounding aims to localize the corresponding region in an image with a specific text description. Following [19], we study weakly-supervised visual grounding without any available bounding box annotations on the RefCOCO+ [40] dataset. We fine-tune our model with global-level image-text alignment tasks (*i.e.*, ITC and ITM) using

Method	VQA		NLVR2	
	test-dev	test-std	dev	test-P
LXMERT [35]	72.42	72.54	74.90	74.50
UNITER _{large} [5]	73.82	74.02	79.12	79.98
OSCAR [21]	73.16	73.44	78.07	78.36
ALBEF [19]	74.54	74.70	80.24	80.50
TCL [38]	74.90	74.92	80.54	81.33
CODIS [9]	74.86	74.97	80.50	80.84
VLC (5.6M) [13]	74.02	74.00	77.70	79.04
MAMO	76.12	76.20	81.86	81.53

Table 3. Comparison with state-of-the-art methods on VQA and NLVR2.

Method	val	testA	testB
ALBEF [19]	58.46	65.89	46.25
MAMO w/o mask	56.61	65.08	42.91
MAMO	61.90	72.30	48.50

Table 4. Weakly-supervised visual grounding results on RefCOCO+.

only image-text supervision. During inference, we utilize Grad-CAM [31] to get image heatmaps and use them to rank the region proposals provided by [39].

4.4. Results on V+L downstream tasks

Results on Image-Text Retrieval. Tables 1 and 2 report the results on fine-tuned and zero-shot image-text retrieval respectively. Our method achieves state-of-the-art (SoTA) performance compared with other methods on all retrieval tasks. On the zero-shot retrieval task, our method outperforms ALBEF [19] by 6.1% on image retrieval R@1 and 8.7% on text retrieval R@1. Although trained with only 4M data, our method even outperforms ALIGN [15] which is trained on a larger amount of 1.8B images. On the fine-tuned setting, we also achieve comparable performance with ALIGN and outperform most previous works trained on a similar amount of data. These superior performances in both zero-shot and fine-tuned retrieval tasks validate that MAMO can generate semantically rich multimodal representations.

ITM+ITC	Tasks			Flickr30K		MSCOCO		VQA test-dev
	MRM	MLM	MIM	TR	IR	TR	IR	
✓				93.5	80.7	71.9	55.2	72.1
✓		✓		93.2	83.7	75.5	58.0	73.9
✓		✓	✓	94.0	83.5	74.7	58.2	74.4
✓	✓			94.1	81.4	71.8	55.5	72.9
✓	✓	✓		95.2	83.6	75.8	59.0	74.6
✓	✓	✓	✓	95.5	84.3	76.6	59.2	74.8

Table 5. Ablation experiments on pre-training tasks. IR: image retrieval recall@1. TR: text retrieval recall@1.

MRM modality	image	Flickr30K		MSCOCO		VQA test-dev
		TR	IR	TR	IR	
		94.0	83.5	74.7	58.2	74.4
✓		93.6	84.4	75.2	58.8	74.7
	✓	94.7	84.2	75.6	58.8	74.7
✓	✓	95.5	84.3	76.6	59.2	74.8

Table 6. Ablation experiments on MRM modalities.

MRM design	Flickr30K		MSCOCO		VQA test-dev
	TR	IR	TR	IR	
MAMO	95.5	84.3	76.6	59.2	74.8
w/o EMA update	×	×	×	×	×
w/o predictor	94.1	83.8	75.6	58.4	74.4

Table 7. Ablation experiments on MRM design. × mean the model diverges during pre-training, leading to terrible performance on downstream tasks.

Results on VQA and NLVR. As is shown in Table 3, our method achieves SoTA performance both on VQA [11] and NLVR2 [34]. Though our method doesn’t use any external object annotations during pre-training, it still outperforms most region-based methods [5, 21] that benefit from object structures in the regional features. Compared to AL-BEF [19], we achieve improvements of 1.50% on VQA test-std and 1.03% on NLVR2 test-P.

Results on Weakly-Supervised Visual Grounding. Table 4 reports the results on weakly-supervised visual grounding. Our method outperforms previous weakly-supervised method [19] and the baseline model pre-trained without masked multimodal modeling. The results suggest that our method helps the model locate semantic regions in images and learn more fine-grained interaction between words and image regions. More visualization examples are shown in Appendix.

4.5. Ablation Study

For ablation studies, we train all models with a shorter training scheduler of 10 epochs. We report R@1 on fine-tuned retrieval tasks and accuracy on VQA.

MIM target	Flickr30K		MSCOCO		VQA test-dev
	TR	IR	TR	IR	
raw pixels	93.1	83.9	75.8	59.1	74.5
visual tokens	95.2	84.0	76.5	58.1	74.6
momentum visual features	95.5	84.3	76.6	59.2	74.8

Table 8. Ablation experiments on MIM prediction targets. We grid search the best decoder depth and report the best results for each variant.

#Blocks	Flickr30K		MSCOCO		VQA test-dev
	TR	IR	TR	IR	
0	95.5	84.3	76.6	59.2	74.8
2	94.7	84.1	75.9	59.3	74.8
4	94.7	84.6	76.1	59.0	74.7
6	95.0	84.2	75.8	59.3	74.7

Table 9. Ablation experiments on MIM decoder depth. 0 refers to a simple MLP projector.

Importance of Pre-training Tasks. We evaluate the effectiveness of our pre-training tasks on Tab. 5. Adding our implicit target MRM on all other tasks brings improvements to almost all downstream tasks. But using MRM alone only slightly improves the performance, which we infer is because the implicit target may collapse into trivial solutions that restrict the modeling capacity, *e.g.*, producing the same values on some feature dimensions. When we combine the implicit MRM with the auxiliary explicit targets, MIM and MLM, the model achieves significantly better performances on both VQA and retrieval tasks, and is also better than using only explicit MLM and MIM targets, suggesting that our implicit and explicit prediction targets are highly complementary.

Influence of MRM Modalities. We explore the separate effects of MRM on vision and language modalities. We compare 4 different MRM settings: 1) without MRM, 2) MRM on image patches only, 3) MRM on text tokens only, and 4) MRM on both image and text. As is shown in Tab. 6, MRM is effective on both modalities. Meanwhile, applying MRM to both modalities simultaneously brings larger performance improvement.

Design Choices of MRM. In Tab. 7, we perform ablation studies on the design details of MRM. When we replace the EMA updating target network with the online network on the last training step, we find MRM loss diverges, resulting in terrible performance on downstream tasks. We argue that the frequent change of prediction targets harms the training process. On the contrary, the EMA updating target network smooths down the prediction targets, leading to a stable learning process. When we remove the asymmetric predictor in MRM, there is a performance degradation on all downstream tasks, which indicates the necessity of the



GT: a little girl in a pink shirt standing near a blue metal sculpture
Input: a little girl in a [mask] [mask] standing near a blue metal sculpture



GT: a man getting ready to kick a soccer ball
Input: a man getting ready to kick a [mask] [mask]

Figure 4. Grad-CAM visualization of MRM on masked text tokens.

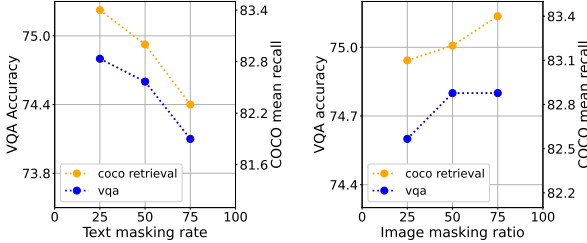


Figure 6. Choices of masking ratio for text and image. The accuracy on VQA test-dev set and the mean recall on MSCOCO retrieval are reported.

predictor since the online representations and target representations are not in the same semantic space.

MIM Prediction Targets. In Tab. 8, we compare different MIM prediction targets including raw pixels, visual tokens, and momentum visual features. We grid search the best decoder depth for each variant. For the raw pixels target, we use a 4-layer transformer decoder. For visual tokens, we use an MLP predictor to predict visual tokens extracted by pre-trained DALL-E [29] codebook. For momentum visual features, we also use an MLP predictor as the decoder. We can see that the high-level momentum visual features target outperforms other low- and mid-level prediction targets.

Decoder Depth of MIM. Some masked image modeling methods such as MAE [14] adopt an asymmetric encoder-decoder architecture. When it comes to MIM with momentum visual features as the target, we also explore whether a decoder is vital to help the model extract better representations. As shown in Tab. 9, we use either transformer or MLP decoder and compare different decoder depths. We find that decoder depth has little influence on our perfor-



an airport filled with planes sitting on tarmacs



a living room with a long couch on it

Figure 5. Grad-CAM visualization of MRM on masked image patches. A deeper color on the word means a higher Grad-CAM value.

mance. Among all these architectures, an MLP layer (depth 0) performs well with the simplest design.

Choices of Masking Ratio. We compare different masking ratios for MAMO on both image and text modalities in Fig. 6. We find that a larger masking ratio on text brings performance degradation while a larger masking ratio on image generally performs better on V+L downstream tasks. We argue that a large masking ratio in the highly compressed text almost destroys the sentence structure. On the contrary, raw images are highly redundant natural signals, requiring a larger masking ratio.

4.6. Visualization

We use Grad-CAM [31] heatmap to showcase the self-attention maps between image and text tokens of the pre-trained model, where the gradients are acquired by minimizing the MRM loss of the masked tokens. We provide the Grad-CAM visualizations for MRM on both masked image patches (MRM-image) and masked text tokens (MRM-text) on the 4th layer of the multimodal fusion encoder. When studying MRM-text, we mask some words in the text and show the Grad-CAM heatmap on the corresponding image. When studying MRM-image, we randomly mask some patches in the image and show the Grad-CAM values on the corresponding text. We provide a few visualizations in Figures 4 and 5. More analysis is in Appendix. The visualization examples show that when MAMO predicts for masked tokens, it tends to put higher attention weights on the semantically correlated tokens in the other modality, indicating fine-grained cross-modal interaction is built during masked multimodal modeling learning.

5. Conclusion

This paper proposes a jointly masked multimodal modeling method to learn fine-grained multimodal representations for VLP. For efficient learning of jointly masked image-text signals, we integrate both implicit and explicit prediction targets that are both high-level and complementary to each other. Extensive experimental results on diverse downstream V+L tasks show that compared to existing methods, our method offers better performance on both zero-shot and fine-tuned settings.

References

[1] Alexei Baevski, Wei-Ning Hsu, Qiantong Xu, Arun Babu, Jitao Gu, and Michael Auli. Data2vec: A general framework for self-supervised learning in speech, vision and language. *arXiv preprint arXiv:2202.03555*, 2022. 3

[2] Hangbo Bao, Li Dong, Songhao Piao, and Furu Wei. Beit: Bert pre-training of image transformers. In *International Conference on Learning Representations*, 2021. 2, 3, 4

[3] Mathilde Caron, Hugo Touvron, Ishan Misra, Hervé Jégou, Julien Mairal, Piotr Bojanowski, and Armand Joulin. Emerging properties in self-supervised vision transformers. In *Proceedings of the IEEE/CVF International Conference on Computer Vision*, pages 9650–9660, 2021. 3

[4] Ting Chen, Simon Kornblith, Mohammad Norouzi, and Geoffrey Hinton. A simple framework for contrastive learning of visual representations. In *International conference on machine learning*, pages 1597–1607. PMLR, 2020. 4

[5] Yen-Chun Chen, Linjie Li, Licheng Yu, Ahmed El Kholy, Faisal Ahmed, Zhe Gan, Yu Cheng, and Jingjing Liu. Uniter: Universal image-text representation learning. In *European conference on computer vision*, pages 104–120. Springer, 2020. 1, 2, 3, 5, 6, 7, 11

[6] Jaemin Cho, Jie Lei, Hao Tan, and Mohit Bansal. Unifying vision-and-language tasks via text generation. In *International Conference on Machine Learning*, pages 1931–1942. PMLR, 2021. 6

[7] Ekin D Cubuk, Barret Zoph, Jonathon Shlens, and Quoc V Le. Randaugment: Practical automated data augmentation with a reduced search space. In *Proceedings of the IEEE/CVF conference on computer vision and pattern recognition workshops*, pages 702–703, 2020. 5

[8] Alexey Dosovitskiy, Lucas Beyer, Alexander Kolesnikov, Dirk Weissenborn, Xiaohua Zhai, Thomas Unterthiner, Mostafa Dehghani, Matthias Minderer, Georg Heigold, Sylvain Gelly, et al. An image is worth 16x16 words: Transformers for image recognition at scale. In *International Conference on Learning Representations*, 2020. 3, 5

[9] Jiali Duan, Liqun Chen, Son Tran, Jinyu Yang, Yi Xu, Belinda Zeng, and Trishul Chilimbi. Multi-modal alignment using representation codebook. In *Proceedings of the IEEE/CVF Conference on Computer Vision and Pattern Recognition*, pages 15651–15660, 2022. 5, 6

[10] Xinyang Geng, Hao Liu, Lisa Lee, Dale Schuurmans, Sergey Levine, and Pieter Abbeel. Multimodal masked autoen-

coders learn transferable representations. *arXiv preprint arXiv:2205.14204*, 2022. 3

[11] Yash Goyal, Tejas Khot, Douglas Summers-Stay, Dhruv Batra, and Devi Parikh. Making the v in vqa matter: Elevating the role of image understanding in visual question answering. In *Proceedings of the IEEE conference on computer vision and pattern recognition*, pages 6904–6913, 2017. 6, 7, 11

[12] Jean-Bastien Grill, Florian Strub, Florent Altché, Corentin Tallec, Pierre Richemond, Elena Buchatskaya, Carl Doersch, Bernardo Avila Pires, Zhaohan Guo, Mohammad Gheshlaghi Azar, et al. Bootstrap your own latent-a new approach to self-supervised learning. *Advances in neural information processing systems*, 33:21271–21284, 2020. 3, 4

[13] Liangke Gui, Qiuyuan Huang, Alex Hauptmann, Yonatan Bisk, and Jianfeng Gao. Training vision-language transformers from captions alone. *arXiv preprint arXiv:2205.09256*, 2022. 3, 6

[14] Kaiming He, Xinlei Chen, Saining Xie, Yanghao Li, Piotr Dollár, and Ross Girshick. Masked autoencoders are scalable vision learners. In *Proceedings of the IEEE/CVF Conference on Computer Vision and Pattern Recognition*, pages 16000–16009, 2022. 2, 3, 4, 8

[15] Chao Jia, Yinfai Yang, Ye Xia, Yi-Ting Chen, Zarana Parekh, Hieu Pham, Quoc Le, Yun-Hsuan Sung, Zhen Li, and Tom Duerig. Scaling up visual and vision-language representation learning with noisy text supervision. In *International Conference on Machine Learning*, pages 4904–4916. PMLR, 2021. 1, 2, 6

[16] Andrej Karpathy and Li Fei-Fei. Deep visual-semantic alignments for generating image descriptions. In *Proceedings of the IEEE conference on computer vision and pattern recognition*, pages 3128–3137, 2015. 11

[17] Jacob Devlin, Ming-Wei Chang, Kenton Lee, and Kristina Toutanova. Bert: Pre-training of deep bidirectional transformers for language understanding. In *Proceedings of NAACL-HLT*, pages 4171–4186, 2019. 2, 3, 5

[18] Ranjay Krishna, Yuke Zhu, Oliver Groth, Justin Johnson, Kenji Hata, Joshua Kravitz, Stephanie Chen, Yannis Kalantidis, Li-Jia Li, David A Shamma, et al. Visual genome: Connecting language and vision using crowdsourced dense image annotations. *International journal of computer vision*, 123(1):32–73, 2017. 5, 11

[19] Junnan Li, Ramprasaath Selvaraju, Akhilesh Gotmare, Shafiq Joty, Caiming Xiong, and Steven Chu Hong Hoi. Align before fuse: Vision and language representation learning with momentum distillation. *Advances in neural information processing systems*, 34:9694–9705, 2021. 1, 2, 5, 6, 7, 11, 16

[20] Liunian Harold Li, Mark Yatskar, Da Yin, Cho-Jui Hsieh, and Kai-Wei Chang. Visualbert: A simple and performant baseline for vision and language. *arXiv preprint arXiv:1908.03557*, 2019. 2, 3

[21] Xiujun Li, Xi Yin, Chunyuan Li, Pengchuan Zhang, Xiaowei Hu, Lei Zhang, Lijuan Wang, Houdong Hu, Li Dong, Furu Wei, et al. Oscar: Object-semantics aligned pre-training for vision-language tasks. In *European Conference on Computer Vision*, pages 121–137. Springer, 2020. 1, 2, 3, 6, 7

[22] Tsung-Yi Lin, Michael Maire, Serge Belongie, James Hays, Pietro Perona, Deva Ramanan, Piotr Dollár, and C Lawrence Zitnick. Microsoft coco: Common objects in context. In *European conference on computer vision*, pages 740–755. Springer, 2014. [5](#), [6](#), [11](#)

[23] Xiao Liu, Fanjin Zhang, Zhenyu Hou, Li Mian, Zhaoyu Wang, Jing Zhang, and Jie Tang. Self-supervised learning: Generative or contrastive. *IEEE Transactions on Knowledge and Data Engineering*, 2021. [4](#)

[24] Ilya Loshchilov and Frank Hutter. Decoupled weight decay regularization. In *International Conference on Learning Representations*, 2018. [5](#), [11](#)

[25] Aaron van den Oord, Yazhe Li, and Oriol Vinyals. Representation learning with contrastive predictive coding. *arXiv preprint arXiv:1807.03748*, 2018. [5](#)

[26] Vicente Ordonez, Girish Kulkarni, and Tamara Berg. Im2text: Describing images using 1 million captioned photographs. *Advances in neural information processing systems*, 24, 2011. [5](#)

[27] Bryan A Plummer, Liwei Wang, Chris M Cervantes, Juan C Caicedo, Julia Hockenmaier, and Svetlana Lazebnik. Flickr30k entities: Collecting region-to-phrase correspondences for richer image-to-sentence models. In *Proceedings of the IEEE international conference on computer vision*, pages 2641–2649, 2015. [5](#), [11](#)

[28] Alec Radford, Jong Wook Kim, Chris Hallacy, Aditya Ramesh, Gabriel Goh, Sandhini Agarwal, Girish Sastry, Amanda Askell, Pamela Mishkin, Jack Clark, et al. Learning transferable visual models from natural language supervision. In *International Conference on Machine Learning*, pages 8748–8763. PMLR, 2021. [1](#), [2](#), [5](#), [6](#)

[29] Aditya Ramesh, Mikhail Pavlov, Gabriel Goh, Scott Gray, Chelsea Voss, Alec Radford, Mark Chen, and Ilya Sutskever. Zero-shot text-to-image generation. In *International Conference on Machine Learning*, pages 8821–8831. PMLR, 2021. [2](#), [3](#), [4](#), [5](#), [8](#)

[30] Shaoqing Ren, Kaiming He, Ross Girshick, and Jian Sun. Faster r-cnn: Towards real-time object detection with region proposal networks. *Advances in neural information processing systems*, 28, 2015. [3](#)

[31] Ramprasaath R Selvaraju, Michael Cogswell, Abhishek Das, Ramakrishna Vedantam, Devi Parikh, and Dhruv Batra. Grad-cam: Visual explanations from deep networks via gradient-based localization. In *Proceedings of the IEEE international conference on computer vision*, pages 618–626, 2017. [2](#), [6](#), [8](#), [11](#)

[32] Piyush Sharma, Nan Ding, Sebastian Goodman, and Radu Soricut. Conceptual captions: A cleaned, hypernymed, image alt-text dataset for automatic image captioning. In *Proceedings of the 56th Annual Meeting of the Association for Computational Linguistics (Volume 1: Long Papers)*, pages 2556–2565, 2018. [5](#)

[33] Weijie Su, Xizhou Zhu, Yue Cao, Bin Li, Lewei Lu, Furu Wei, and Jifeng Dai. Vl-bert: Pre-training of generic visual-linguistic representations. *arXiv preprint arXiv:1908.08530*, 2019. [1](#), [2](#)

[34] Alane Suhr, Stephanie Zhou, Ally Zhang, Iris Zhang, Hua-jun Bai, and Yoav Artzi. A corpus for reasoning about natural language grounded in photographs. In *Proceedings of the Annual Meeting of the Association for Computational Linguistics*, 2019. [6](#), [7](#), [11](#)

[35] Hao Tan and Mohit Bansal. Lxmert: Learning cross-modality encoder representations from transformers. In *Proceedings of the 2019 Conference on Empirical Methods in Natural Language Processing and the 9th International Joint Conference on Natural Language Processing (EMNLP-IJCNLP)*, pages 5100–5111, 2019. [2](#), [6](#)

[36] Chen Wei, Haoqi Fan, Saining Xie, Chao-Yuan Wu, Alan Yuille, and Christoph Feichtenhofer. Masked feature prediction for self-supervised visual pre-training. In *Proceedings of the IEEE/CVF Conference on Computer Vision and Pattern Recognition*, pages 14668–14678, 2022. [3](#)

[37] Zhenda Xie, Zheng Zhang, Yue Cao, Yutong Lin, Jianmin Bao, Zhuliang Yao, Qi Dai, and Han Hu. Simmim: A simple framework for masked image modeling. In *Proceedings of the IEEE/CVF Conference on Computer Vision and Pattern Recognition*, pages 9653–9663, 2022. [3](#), [4](#)

[38] Jinyu Yang, Jiali Duan, Son Tran, Yi Xu, Sampath Chanda, Liqun Chen, Belinda Zeng, Trishul Chilimbi, and Junzhou Huang. Vision-language pre-training with triple contrastive learning. In *Proceedings of the IEEE/CVF Conference on Computer Vision and Pattern Recognition*, pages 15671–15680, 2022. [5](#), [6](#)

[39] Licheng Yu, Zhe Lin, Xiaohui Shen, Jimei Yang, Xin Lu, Mohit Bansal, and Tamara L Berg. Mattnet: Modular attention network for referring expression comprehension. In *Proceedings of the IEEE Conference on Computer Vision and Pattern Recognition*, pages 1307–1315, 2018. [6](#), [11](#)

[40] Licheng Yu, Patrick Poirson, Shan Yang, Alexander C Berg, and Tamara L Berg. Modeling context in referring expressions. In *European Conference on Computer Vision*, pages 69–85. Springer, 2016. [6](#), [11](#)

[41] Pengchuan Zhang, Xiujun Li, Xiaowei Hu, Jianwei Yang, Lei Zhang, Lijuan Wang, Yejin Choi, and Jianfeng Gao. Vinvl: Revisiting visual representations in vision-language models. In *Proceedings of the IEEE/CVF Conference on Computer Vision and Pattern Recognition*, pages 5579–5588, 2021. [2](#)

[42] Jinghao Zhou, Chen Wei, Huiyu Wang, Wei Shen, Cihang Xie, Alan Yuille, and Tao Kong. Image bert pre-training with online tokenizer. In *International Conference on Learning Representations*, 2021. [2](#), [3](#), [4](#)

A. Details on Fine-tuning for Downstream Tasks

For all downstream tasks, we use AdamW [24] optimizer with a weight decay of 0.01 and a linear learning rate scheduler. All downstream tasks take images with a 384×384 resolution as inputs.

Image-Text Retrieval. We fine-tune our model on two retrieval datasets: MSCOCO [22] and Flickr30K [27]. We split the two datasets into train / val / test sets separately following the widely-used Karpathy split [16]. We fine-tune our model for 10 epochs with a batch size of 160 and an initial learning rate of 3×10^{-5} , optimizing the ITC and ITM loss. During inference, we select the top- k (256 for MSCOCO, and 128 for Flickr30K) candidates using ITC scores and calculate their ITM scores to rank these candidates following [19].

Visual Question Answering (VQA). Following previous methods [19], we use both train and validation sets in VQA2.0 dataset [11] and the question-answer pairs from Visual Genome [18] for training. Our VQA model uses a cross-attention decoder to generate answers. We initialize the decoder using the weights from our pre-trained multimodal fusion encoder and fine-tuning the VQA model for 10 epochs with a batch size of 192 and an initial learning rate of 5×10^{-5} , optimizing the conditional language-modeling loss. To fairly compare with other methods, we constrain the decoder output to only generate 3,129 candidate answers during inference. Performance on the test-dev and test-std splits are reported.

Natural Language for Visual Reasoning (NLVR). We evaluate our model on NLVR2 dataset [34]. In NLVR task, the model receives one text and two input images. Since our model only handles one image and one text, we combine each image with the text to create two image-text pairs and extract their multimodal representations separately. Following [5], we use a bi-attention module to fuse the above two multimodal representations. We attach an FC layer to the concated bi-attention pair to get the result score for true-or-false classification. We fine-tune the NLVR model for 10 epochs with a batch size of 80 and an initial learning rate of 3×10^{-5} .

Visual Grounding. We fine-tune our weakly-supervised visual grounding model on RefCOCO+ dataset [40]. We use global-level image-text alignment tasks (ITC and ITM) to train the model while removing random cropping. We fine-tune the model for 5 epochs with a batch size of 160 and an initial learning rate of 2×10^{-5} . During inference, we use ITM loss to calculate Grad-CAM [31] heatmap on

the 4th self-attention layer in the multimodal fusion encoder. And we use the Grad-CAM value to select the best bounding box provided by [39].

B. Pre-training Dataset Details

Table 10 shows the statistics of the pre-training datasets.

	MSCOCO	VG	SBU	CC-3M
#image	113K	100K	860K	2.95M
#text	567K	769K	860K	2.95M

Table 10. Statistics of the pre-training datasets.

C. Visualization of Visual Grounding

In Fig. 7, we show the grounding heatmap of our model in weakly-supervised visual grounding. Meanwhile, we also show the heatmap given by a baseline model pre-trained without masked multimodal modeling. The heatmaps are based on Grad-CAM [31] on the 4th layer of the multimodal fusion encoder, calculated by ITM loss.

D. Visualization of Visual Question Answering

In Fig. 8, we show the Grad-CAM heatmap on the last layer of the multimodal encoder in our VQA model.

E. Additional Visualization Examples for MRM

In Figs. 9 and 10 we show more visualization examples of MRM on masked image patches and text tokens. Heatmaps on images and weights on texts are based on Grad-CAM [31] on the 4th layer of the multimodal fusion encoder.

F. Visualization of Per-word Localization

In Figs. 11 to 13, we show the Grad-CAM heatmap for each word in texts. It's worth noting that our MAMO can localize each word concept more precisely and comprehensively comparing with ALBEEF. Instead of only focusing on some scattered small regions, MAMO more finely localizes the whole objects, showing a solid ability to separate different objects.



Figure 7. Grad-CAM visualization of weakly-supervised visual grounding. Given an image-text input, we compare the image’s Grad-CAM heatmap between a baseline model without masked multimodal modeling (the middle image) and our MAMO model (the right image). Compared with the model without masked multimodal modeling, MAMO can localize relevant regions more precisely. For example, MAMO can recognize the mentioned object, color and number of the text description in the image.

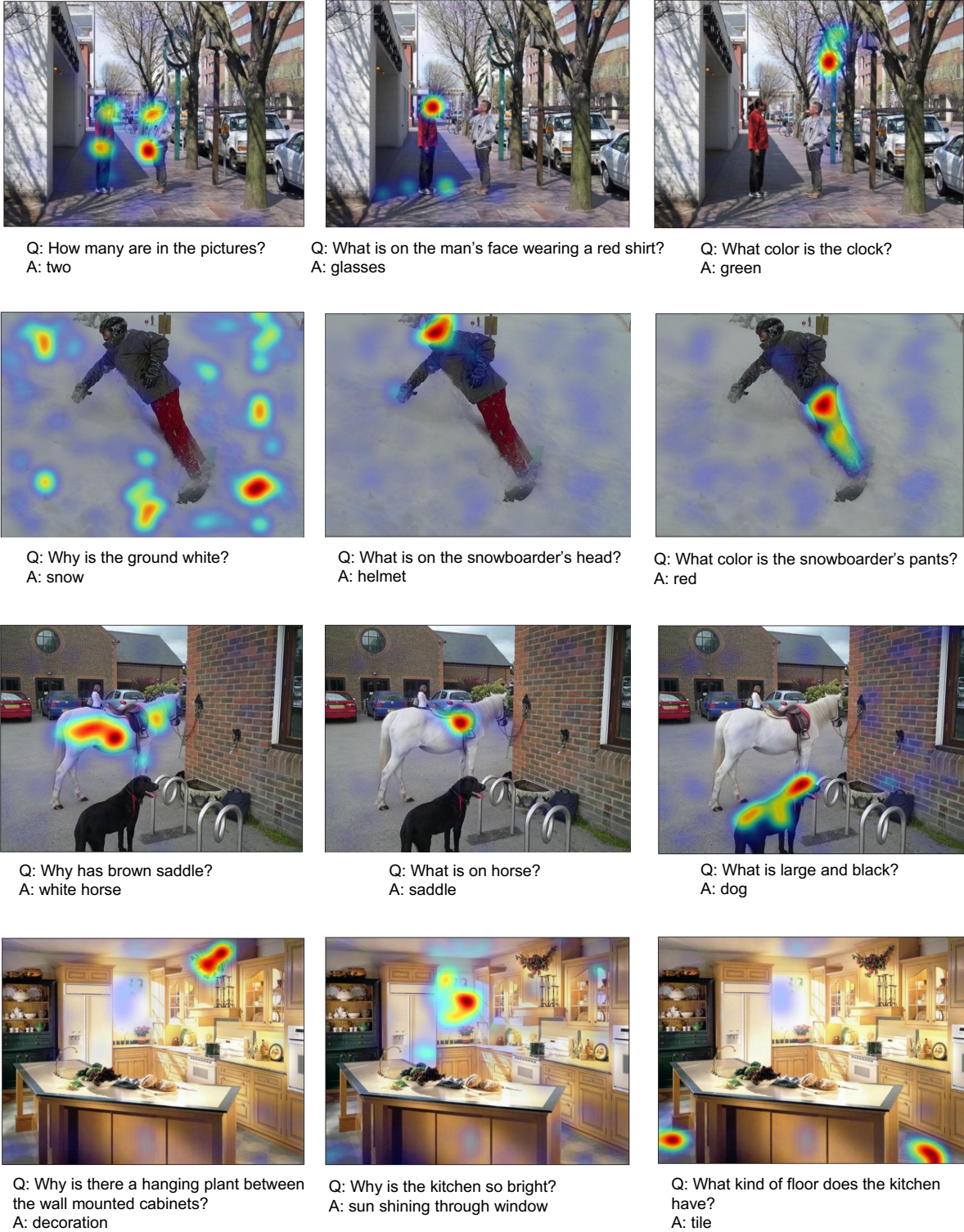
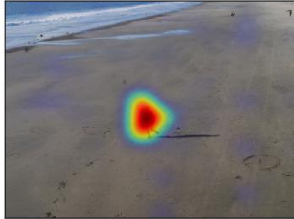


Figure 8. Examples of Grad-CAM visualization on VQA. MAMO can pay attention to the related image regions that helps to determine the answer.



GT: a person on the beach next to the ocean
Input: a [mask] on the beach next to the ocean



GT: a giraffe checking out the bark on a tree
Input: a [mask] checking out the bark on a tree



GT: a messy and unmade bed and a red chair
Input: a messy and unmade bed and a [mask] [mask]



GT: a gray cat laying on top of a wooden book shelf
Input: a gray cat [mask] [mask] [mask] of a wooden book shelf



GT: a small glass filled with alcohol sitting on a table
Input: a small glass filled with [mask] sitting on a table



GT: old luggage cases one is brown and one is green
Input: old luggage cases one is [mask] and one is green



GT: a tall stone building with a massive clock on its side
Input: a tall stone building with a [mask] [mask] on its side



GT: old luggage cases one is brown and one is green
Input: old luggage cases one is brown and one is [mask]

Figure 9. More examples of Grad-CAM visualization of MRM on masked text tokens. MAMO can localize the specific image regions that correspond to the masked words, implying fine-grained image-text interactions are built. Moreover, MAMO not only pays attention to objects (e.g. “chair”) but also attributes (e.g. “brown”) and relations (e.g. “on top of”).

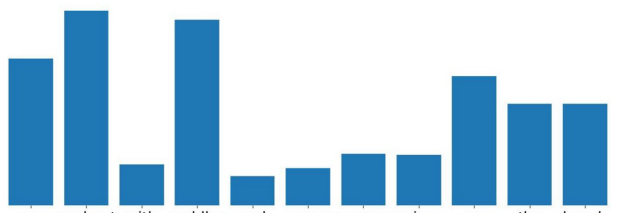
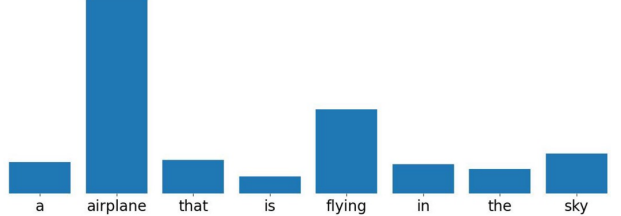
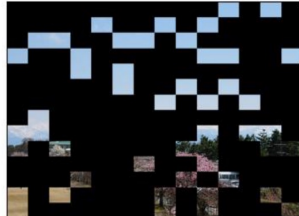
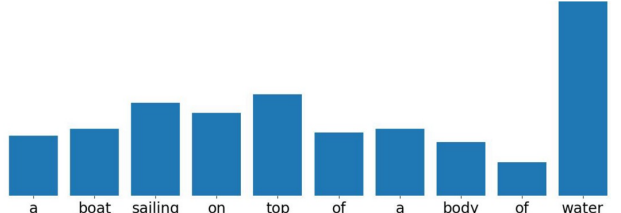
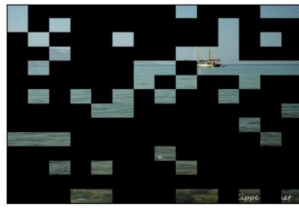
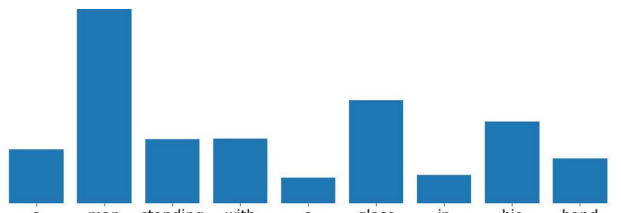
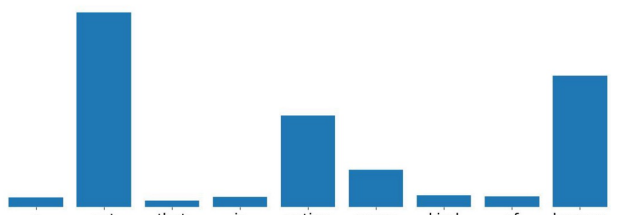
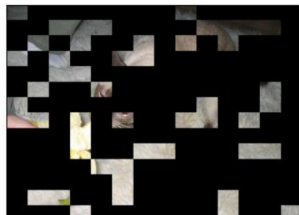
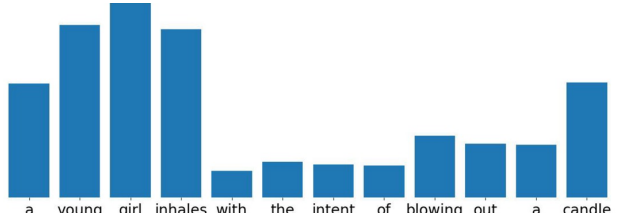
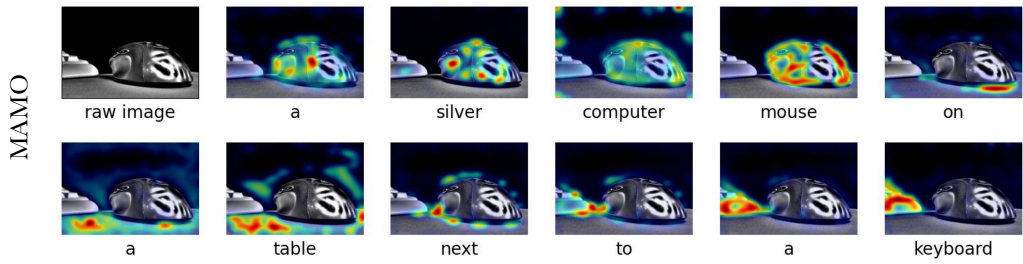
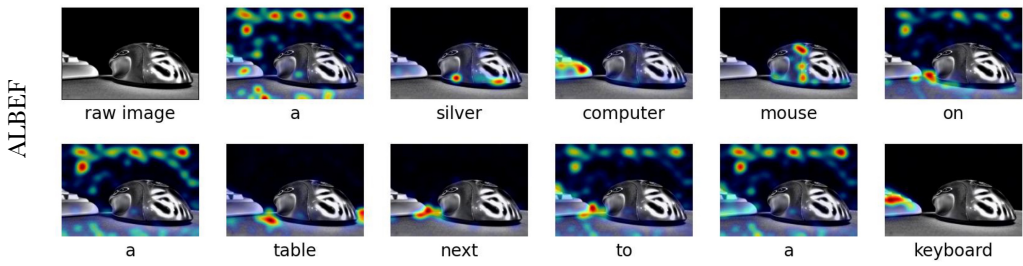
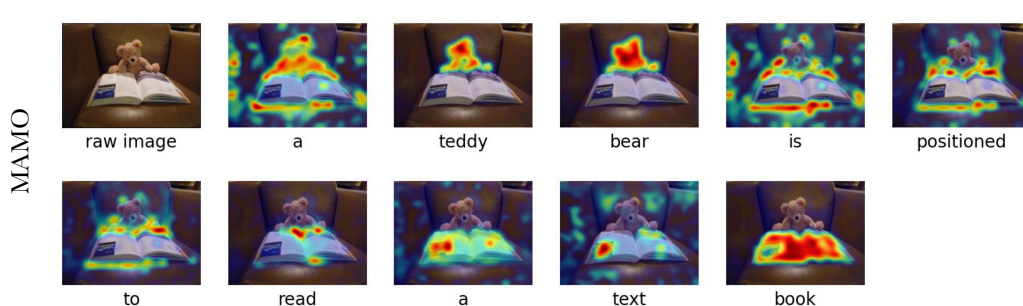
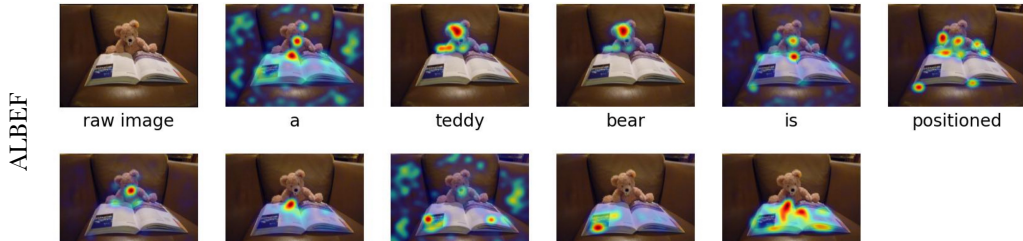


Figure 10. More examples of Grad-CAM visualization of MRM on masked image patches. We show each word token’s Grad-CAM value in the histogram. MAMO pays more attention to words that correspond to the masked image patches.

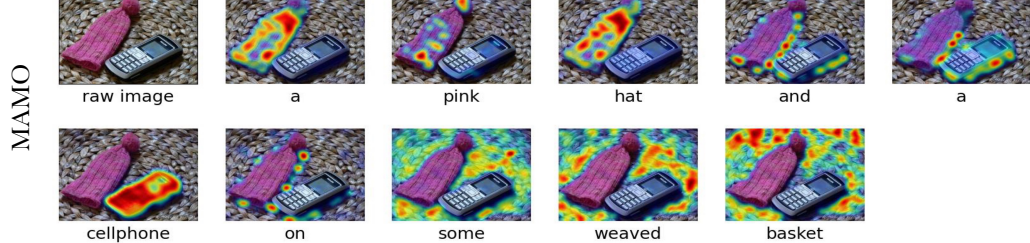


Caption: a silver computer mouse on a table next to a keyboard

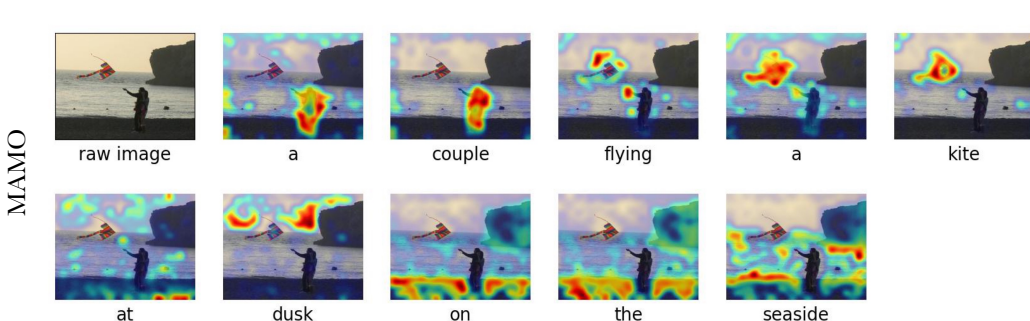
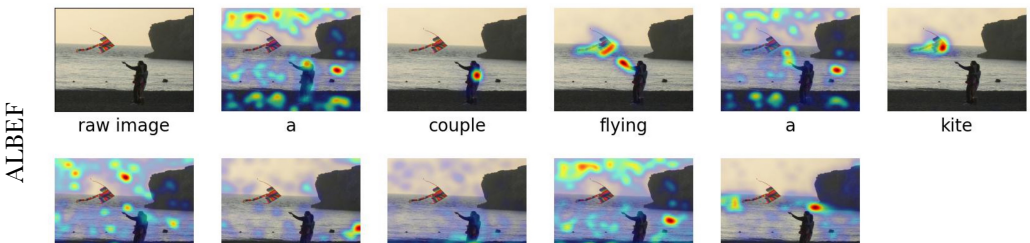


Caption: a teddy bear is positioned to read a text book

Figure 11. Examples of per-word Grad-CAM visualization. MAMO can localize each word concept more precisely and comprehensively comparing with ALBEF [19]. Instead of only focusing on some scattered small regions, MAMO more finely localizes the whole objects, showing a solid ability to separate different objects.

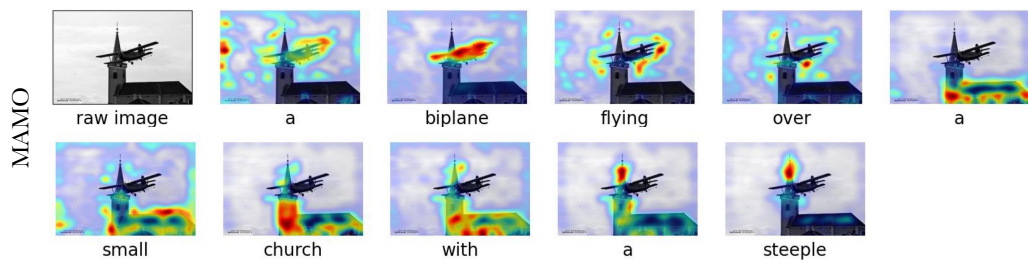
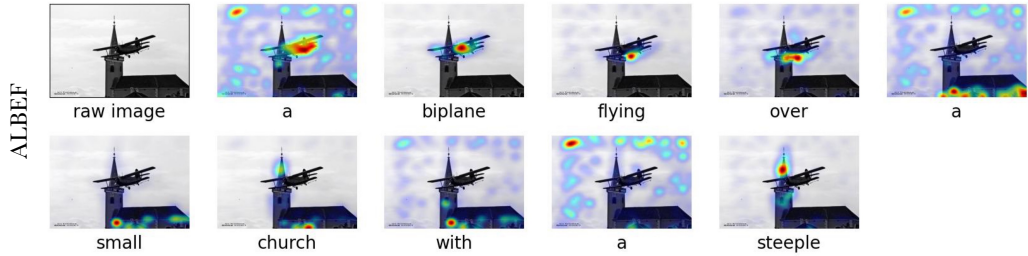


Caption: a pink hat and a cellphone on some weaved basket



Caption: a couple flying a kite at dusk on the seaside

Figure 12. Examples of per-word Grad-CAM visualization.



Caption: a biplane flying over a small church with a steeple



Caption: a traffic motorcycle cop waits to give a ticket

Figure 13. Examples of per-word Grad-CAM visualization.